AIAA Propulsion and Energy Forum
19-22 August 2019, Indianapolis, IN
AIAA Propulsion and Energy 2019 Forum

10.2514/6.2019-4079

Time-varying non-classical electron resistivity in a hollow cathode plume

Marcel P. Georgin,* Benjamin A. Jorns,† and Alec D. Gallimore ‡
University of Michigan, Ann Arbor, MI, 48109

An investigation is performed into the time-dependent correlation between the local electron resitivity in a hollow cathode plume and the enhanced electron drag induced by wave-driven turbulence. Emissive, floating, and ion saturation current probes are applied to the plume of a 20-A class LaB6 hollow cathode to characterize the density, potential, and electron temperature. Emissive probes are employed to characterize the energy in ion acoustic turbulent modes near the cathode exit plane. The actual electron resistivity in the cathode plume is measured through a solution of the generalized Ohm's law with the measured plasma properties. The energy in the ion acoustic turbulence is related to an enhanced resistivity on the electrons through a quasilinear formulation. A phase-averaging technique is applied to both sets of measurements to generate spatially resolved maps of the total resistivity and wave-driven contribution on the time scale of the 45 kHz, large-scale plume mode oscillation in the cathode plasma. The time-averaged values of the plasma properties show that, as is consistent with previous numerical simulations, the electron resistivity in the cathode plume is greater than two orders of magnitude higher than electron resistance and can be explained entirely by the wave-driven turbulence. The wave-driven drag similarly is the dominant contributor to electron resistance on the time-scale of the 45 kHz oscillations in the near-field of the cathode. These results suggest that the quasilinear form for the turbulence driven transport is correct for both the time-averaged and time-resolved dynamics in the plume. These results are discussed in the context of the relationship between the ion acoustic turbulence and the onset of the plume mode oscillation.

I. Nomenclature

E	=	Electric field
n	=	Plasma density
m_e	=	Electron mass
m_i	=	Ion mass
M_e	=	Electron mach number
T_e	=	Electron temperature
u_e	=	Electron drift velocity
W	=	Wave energy
ν	=	Total collision frequency
ν_{an}	=	Anomalous collision frequency
ν_{ion}	=	Ionization frequency
Φ	=	Potential
ϕ	=	Phase
ω	=	Frequency

II. Introduction

Plasma oscillations and turbulence are known to play a vital role in establishing the plasma state in the plumes of hollow cathodes that are used as electron sources for electric propulsion systems. As greater lifetime and performance

*Ph.D. Candidate, Applied Physics, and AIAA Student Member.
†Associate Professor, Aerospace Engineering, and AIAA Senior Member.
‡Professor, Aerospace Engineering, and AIAA Fellow.

is demanded from these propulsion systems for new, ambitious missions, so too is there a need for a better understanding of the underlying unsteady processes that are thought to dictate cathode performance and lifetime. To date, however, our limited understanding of the fundamental physics driving these instabilities prevents us from predicting their onset as well as long-term effects on cathode and, ultimately, thruster performance metrics. These potential risks have compelled a recent investigation into the physics of hollow cathodes through experiment, theory and modeling[1–10].

The initial investigation of hollow cathode physics focused on non-classical effects of ion acoustic turbulence (IAT), an electrostatic drift instability that onsets when the electron velocity exceeds the ion sound speed [11]. The dominant, non-classical effect is the collisionless scattering of electrons off ion sound waves, whereby the electron momentum is resonantly donated to the wave, resulting in growth of the instability. This kinetic effect on the electrons can be represented in a fluid description through an anomalous collision frequency that enhances the classical electron collision frequency [12, 13]. This non-classical term results in an increased plasma resistivity and Ohmic heating, which can be determined from properties of the turbulence and background plasma parameters. The inclusion of this effect in numerical models is necessary to yield agreement with experimental measurements of the steady-state plasma parameters. [5, 7–9].

In addition to improved fidelity, the inclusion of this anomalous resistivity in numerical models also can give rise to a large-scale, low-frequency plasma instability in simulations of cathodes [8, 9]. The authors of these codes correlated the onset of this wave with the effect of anomalous resistive heating of electrons from turbulence, and they have interpreted it as an ionization instability driven by non-classical heating of electrons by the IAT. Qualitatively, the simulations reflect experimental measurements of a large-scale instability sometimes present in hollow cathode discharges, the so-called plume mode instability [3, 14–20]. This plume mode is characterized by quasi-coherent fluctuations in density, potential, and light emission that lead to a dramatic rise in the erosion rate and discharge voltage. While it is known, empirically, that this mode can be driven unstable by reducing the flow rate to the cathode at constant current, an onset criterion from first principles still remains elusive. It thus to date has not been possible to predict the onset of this mode. Given its deleterious effects on cathode operation, this inability poses a risk to developing and flight qualifying systems for long-duration missions.

In light of this operational challenge, we have explored both theoretically and experimentally in recent work the nature of the plume mode instability [17–20]. In previous work, it has been shown that the resistivity of the cathode plume is dominated by ion acoustic turbulence [6, 21]. More recently, we have showed that the large-scale oscillations in density and light emission are highly correlated in space and time with oscillations in the amplitude of the underlying IAT [20]. Linking these two previous results together, others have proposed that the dependence of the resistivity on the IAT may in fact drive the plume mode [8, 9]. Sary [8] showed that large potential, density and temperature fluctuations are generated near the cathode orifice and propagate as coherent structures and Mikellides [9] found that there was an "active region" near the edge of the plasma plume where low-frequency density oscillations, commensurate with the ionization rate, existed. In both cases, as a critical tenet to this hypothesis, it has been suggested that the anomalous resistivity from the IAT must vary on the time-scale of the plume mode oscillations and in turn that this anomalous resistivity can be represented by simple scaling laws. While these modeling results are promising in that they exhibit oscillations that share quantitative features in common with the plume mode oscillation, there has yet to be experimental evidence demonstrating this time-resolved correlation. Absent experimental evidence, it thus remains an open question as to the role of IAT in the onset of the plume mode. As an initial step in evaluating this process, there is a pressing need to confirm if the resistivity remains anomalous on the time-scale of the plume mode oscillations and to determine if the wave-driven contributions are in keeping with the simple expressions used in previous modeling results. To this end, in this investigation, we focus on measure experimentally the wave-driven electron resistivity during a period of the plume mode oscillations.

This article is organized in the following way. First, we provide an overview of the methods for calculating the electron collision frequency and the effective collision frequency from IAT. Then we discuss the experimental setup, including details on the probe diagnostics use to estimate plasma parameters. Following is a presentation of the time-average measurements of plasma and wave properties. The time-resolved measurements are used to correlate fluctuation in the small-scale turbulence with the electron collision frequency to show that fluctuations in the turbulence level are indeed the root cause of the oscillations in plasma resistivity and likely result in the coherent plume mode oscillations.

III. Methods for Estimating Total and Wave-driven Resistivity in the Hollow Cathode Plume

In this section we discuss the methods used for calculating the anomalous collision frequency in the plume of the hollow cathode. We determine this quantity in two ways, one from a momentum balance and another from turbulence properties. A comparison of these two result is then used in the following sections to show the importance of the fluctuations wave-driven collisions in the time-resolved total collision frequency.

First, we examine a fluid formulation for determining the anomalous collision frequency. By neglecting the electron inertia and assuming the ion drift is small compared to the electrons, we arrive at an Ohm's law for electron momentum

$$0 = -nqE - \nabla(nqT_e) - nm_e u_e \nu_e \,, \tag{1}$$

where n is the density, q is the unit charge, E is the electric field, T_e is the electron temperature in eV, m_e is the electron mass, u_e is the electron velocity, and ν_e is total electron collision frequency. Given the known effects of IAT on the electron collision frequency, we treat the total electron frequency as being composed of three parts $\nu_e = \nu_{cl} + \nu_{en} + \nu_{an}$. The classical Coulomb collision frequency, ν_{cl} is given by [22]

$$\nu_{cl} = 2.91 \times 10^{-12} n \lambda_{ei} T_e^{-3/2} \,, \quad \text{where} \quad \lambda_{ei} = 23 - \frac{1}{2}\ln\left(\frac{nT_e^3}{10^6}\right) \,, \tag{2}$$

the electron-neutral collision frequency, ν_{en}, is calculated from an empirical cross section [23] and

$$\nu_{en} = n_n \sigma_{en}(T_e) v_e \,, \tag{3}$$

where n_n is the neutral plasma density and v_e is the electron thermal speed. Through these equations, the anomalous contribution, ν_{an}, that is due to the effective drag turbulence can be calculated. From Eqns. 1 - 3, we can determine the anomalous component to the electron collision frequency, provided we know the density, the electric field, and the electron temperature and electron drift velocity.

Alternatively, we can estimate the anomalous collision frequency from the quasi-linear theory of IAT. The momentum lost by electrons is due to collisionless momentum exchange with each mode in the IAT spectrum [13]. Therefore we can balance rate at which momentum is lost by electron to the rate at which the wave gains momentum, or

$$nm_e u_e \nu_{an}^{IAT} = \sum_k p_k \gamma_k \,, \tag{4}$$

where p_k is the momentum density of and IAT wave with wavevector k and γ_k is the temporal growth rate of an IAT mode. Physically, this equation implies that the greater the growth in the IAT, the faster momentum is removed from the electrons and transferred to the wave. Furthermore, the more IAT modes there are in the plasma, the more momentum can be transferred out of the electron fluid to the turbulence. To evaluate this expression we define the momentum of each mode as [13]

$$p_k = W_k \frac{k}{\omega_r} \,, \tag{5}$$

where W_k is the wave energy density of the IAT and ω_r is the real component of the frequency. Applying the dispersion in the large wavelength limit and the quasi-linear growth rate for kinetically driven IAT[11], it can be shown that [13]

$$\nu_{an}^{IAT} = \sum_k \sqrt{\frac{\pi}{2}\frac{m_i}{m_e}}\omega_k \left(\frac{q\phi_k}{T_e}\right)^2 \,. \tag{6}$$

Through Eqn. 6, we can estimate the anomalous collision frequency from IAT if we are able to measure the electron temperature and plasma potential fluctuations.

In numerical models, the effects of IAT are often included through a closure model for the anomalous collision frequency that is based on the background plasma parameters. Mikellides et al. [9] use a closure based on the saturation of the IAT through non-linear wave-particle interactions

$$\nu_{an} = \alpha \frac{T_e}{T_i}\omega_{pi}\frac{u_e}{c_s} \,, \tag{7}$$

where ω_{pi} is the ion plasma frequency, T_i is the ion temperature, c_s is the ion sound speed, and α is a scaling parameter derived from the decay of the IAT Fourier spectrum at high frequency[24]. Alternatively, Sary et al. [7, 8] allows for growth and convection of the IAT. For our purposes of evaluating this closure, we will neglect the convection.

$$\nu_{an} \propto \alpha\omega_{pe}\frac{W}{nT_e}, \qquad \frac{\partial W}{\partial t} = \frac{2}{9}\frac{m_e}{m_i}\omega_{pe}\sqrt{\pi}\sqrt{\frac{3}{2}}(M_e - 1)\,, \tag{8}$$

where W is the wave energy density of the turbulence, and M_e is the electron Mach number. We examine these two closures in later sections by evaluating them with our measurements of the background plasma parameters.

Using these two methods for calculating the anomalous collision frequency, one from the fluid equations another from IAT theory, we evaluate the hypothesis that the IAT is driving the time-average resistivity as well as its fluctuations in the plasma. Furthermore we will examine the closure models used by Mikellides [9] and Sary[8]. In the following section, we discuss the experimental techniques we used to measure the plasma density, electron temperature, electron drift, electric field, and high-frequency turbulence as a function of position and time in the plume of a hollow cathode.

IV. Experimental Methods

We conducted our experiments using a 20 A hollow cathode with a LaB_6 insert, 3 mm tungsten orifice, and a graphite keeper electrode. The plasma discharge was established between the cathode and a cylindrical tungsten anode located 70 mm downstream of the keeper surface. We operated the cathode at 20 A, 5 sccm Xe, and 36 V of discharge voltage – a plume mode condition. The cathode was operated in a 0.5 m × 1 m vacuum chamber at a background pressure of 20 μTorr-Xe. The experimental configuration is shown in Fig. 1 where the cathode, anode and probe are visible.

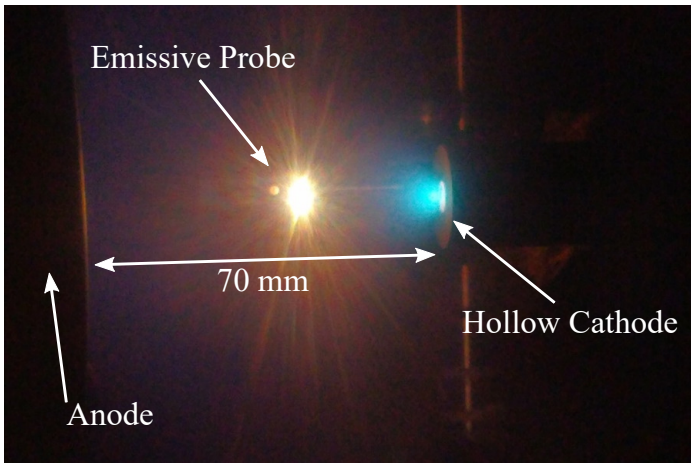

Fig. 1 20 A hollow cathode operating with 5 sccm of Xe, a plume mode condition.

We use electrostatic probes to measure oscillations in plasma potential, floating potential, and ion saturation current. The plasma potential is measured with an emissive probe (shown in Fig. 1), which was constructed with 0.13 mm thoriated tungsten wire. The signal was measured at 12.5 MHz using an oscilloscope. The floating potential was measured with a cylindrical probe 2 mm long with a 0.13 mm diameter. We note that because the cathode-to-ground voltage differed after switching probes and that we corrected for this by subtracting the difference in cathode-to-ground from the floating probe measurement. We used the same probe, biased to -54 V, and a 100 Ohm low-inductance shunt resistor to measure the oscillations in ion saturation current at 10 MHz with an oscilloscope. We also simultaneously collected discharge current waveforms using the oscilloscope and a high-speed Hall probe. This signal acts as a reference to conduct a phase-average of these plasma parameters in post-processing. This analysis allows us to examine the evolution of these plasma parameters over a single cycle of the discharge current oscillation. Additional details on the analysis is provided in Sec.V. By translating the probe, we were able to measure the evolution of these parameters in time and space.

We note that the presence of electrostatic probes in a plasma is often perturbative and this experiment is no exception. In particular, when a probe was placed near the cathode, the discharge voltage changes and the waveform of the discharge

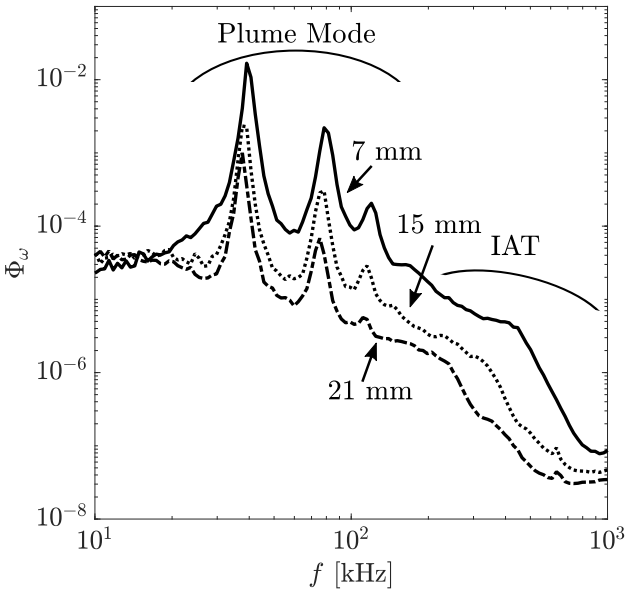

Fig. 2 Fourier transform of the plasma potential signal normalized to the electron temperature at three positions in the plume.

current oscillations can as well. While the discharge current and flow rate were kept constant, the discharge voltage changed by up to 3 V depending on which probe was present in the plasma and its position. As such, we only present results where the characteristic waveform of the plume mode was clearly visible in the discharge current.

V. Results

Although numerical models of cathodes suggest that Ohmic heating from IAT is the driver for the plume mode instability, there are no experimental measurements that directly show that the observed resistivity is equal to the anomalous resistivity predicted by turbulence theory. Our goal is to show this relationship by calculating the anomalous collision frequency from Eqn. 1 and the classical parameters such as density, velocity, temperature, and electric field and comparing with the effective collision frequency calculated from measurements of high-frequency modes and Eqn. 6. Through our investigation, we first compare the time-average anomalous collision frequency from both methods then we examine its evolution in time.

A. Time-average Anomalous Resistivity and High-frequency Turbulence

Figure 2 shows the Fourier decomposition of the emissive probe signal normalized to its time-average value (relative plasma potential fluctuations) at three positions in the plume. Here, we see the large scale, low-frequency oscillations of the plume mode at 45 kHz and its harmonics as well as the broadband high-frequency turbulence associated with the IAT beyond 150 kHz. We find that the spectral power decreases with increasing position away from the cathode.

The emissive probe directly gives us the plasma potential, Φ, which we use to calculate the electric field, E, as

$$E = -\nabla\Phi \, . \tag{9}$$

Combining the emissive probe and ion saturation probe with cylindrical probe theory, we can calculate the electron temperature as

$$T_e = 2\frac{\Phi - V_f}{\ln\left(\frac{1}{2\pi}\frac{m_i}{m_e}\right)} \, , \tag{10}$$

where Φ is the plasma potential and V_f is the floating potential. Figure 3a shows the time average evolution these parameters along the axis of the discharge. Here, we have fit the data with a smoothing spline for smoother gradients in

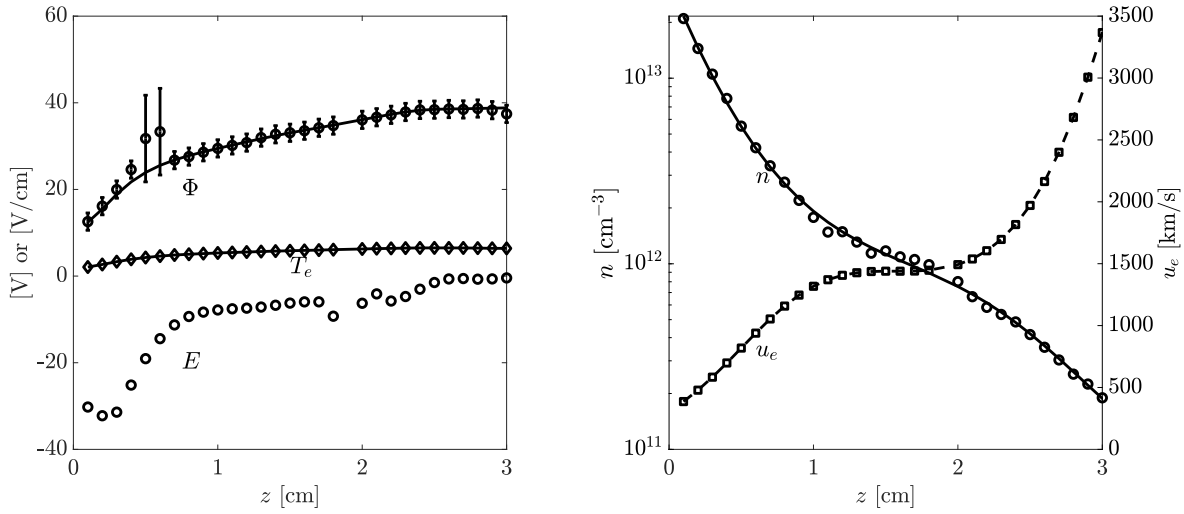

(a) The time-averaged potential, electric field, and electron temperature as a function of position.

(b) The time-averaged density and velocity as a function of position.

Fig. 3 Time-average plasma parameters

potential to calculate the electric field. The uncertainty is larger on two points in Fig. 3a because the cathode would mode hop, resulting in large, abrupt changes in the measured plasma potential and fluctuations when the probe was at these positions. Figure 3a shows a sharp $\sim$ 10 V increase near the cathode and a slow rise in potential towards the anode. These trends have corresponding features in the electric field. This stark rise in potential has been noted before in experiment and simulation and has been attributed to non-classical electron resistivity [3, 6, 25, 26]. On the other hand, the electron temperature rises slowly in the plume from 2 eV to 6 eV.

Once we have calculated the electron temperature, we can then use the ion saturation current to find the plasma density using

$$n = \frac{I_{sat}}{q c_s A_p}\,, \tag{11}$$

where $c_s = \sqrt{qT_e/m_i}$ is the ion sound speed, A_p is the probe surface area, and q is the unit charge. Furthermore, by combining our temperature measurement with a model for the low energy ionization cross section of xenon [27] and an approximation of the neutral density, n_n, in the plume we determine the ionization rate, $\nu_{ion}(T_e)$. Here, we model the neutrals as a conically expanding gas following Ref. [27]

$$n_n(z) = \frac{\dot{m}}{m_i v_n \pi \left(r_k + \alpha z\right)^2}, \tag{12}$$

where $\dot{m}$ is the xenon flow rate, v_n is the neutral thermal velocity, r_k is the keeper radius, and we have used $\alpha = 1$, corresponding to a 45° half angle of expansion. Having calculated these two parameters, density and ionization rate, we can then find the electron drift velocity, u_e, by numerically integrating the electron continuity equation. We do not have 2D measurements of density and temperature that would be necessary to estimate electron density from the continuity equation. In lieu of this, we instead make a quasi 1D approximation that the plasma expands conically and with constant density and temperature at each axial cross-section. The expression used in our analysis is

$$A(z) = \pi \left(r_k + \alpha z\right)^2\ . \tag{13}$$

Here, we have used $\alpha = 0.4$, which is consistent with the plasma expanding from the keeper orifice to the anode radius. This approximation is consistent with the work done in Ref. [9] and experimental observations of hollow cathodes reported in Ref. [6]. Subject to this approximation, if we denote the changing cross sectional area, $A(z)$, of the plasma, we can estimate the electron velocity along centerline, u_e as

$$u_e = \frac{\int_0^z (n\nu_{ion} - \frac{\partial n}{\partial t}) A(z) dz}{A(z) n} + \frac{n(0,t)}{n}\frac{A(0)}{A(z)} u_e(0,t)\,. \tag{14}$$

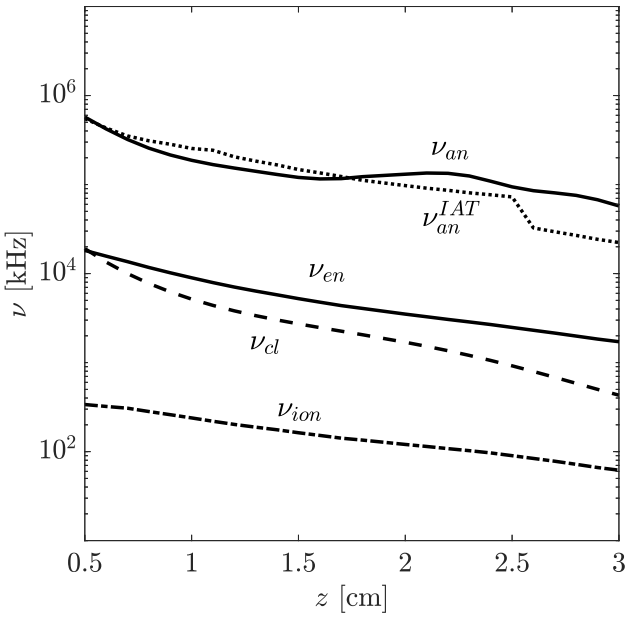

Fig. 4 The time-averaged anomalous collision frequency, classical collision frequency, ionization frequency, and the anomalous collision frequency from IAT.

For this calculation, we employ a boundary condition at the keeper orifice where we use the discharge current and the keeper orifice diameter, A_k to determine the initial electron velocity through $u_e(0,t) = I_{dc}(t)/(n(0,t)qA_k)$. Figure 3b shows the time average density and velocity profiles along the axis of the discharge. We see that the density decreases monotonically along the axis of the discharge by nearly two orders of magnitude whereas the velocity increases by a factor of 7. We note that we have fit $\log(n)$ with a 5^{th} order polynomial (solid line) for smooth gradients. Between 1 and 2 cm, the electron velocity increases more slowly. This occurs because in this region, the first term in Eqn. 14 has become negligible (the ionization rate and density are low) and the density (who's gradient is reduced between 1 and 2 cm) and the cross-sectional area happen to be changing almost exactly inversely to each other, leaving the second term nearly constant with position. Because the density gradient becomes more negative beyond 2 cm, the velocity begins to increase once more. This is to say, the feature in the velocity is due to the changes in the gradient in density and its presence is not sensitive to the angle of of the expansion, α. From these parameters, n, u_e, E, and T_e, we can evaluate the electron momentum equation, Eqn. 1, to solve for the electron collision frequency.

Alternatively, we can determine the anomalous collision frequency from Eqn. 6 and our measurements of high-frequency turbulence (see Fig. 2). We restrict our sum over electrostatic plane waves to those associated with the IAT ($f > 150$ kHz). Figure 4 shows the result of these collision frequency analyses along with the ionization frequency. Note we have truncated the domain because in the near field (0-0.5 cm), the probe was too perturbative and gave unrealistic results for the high-frequency energy content. Examining this figure, first we find that all the characteristic frequencies decrease with increasing position. We also confirm the results of others, showing that the non-classical collision frequency is orders of magnitude higher than its classical counterpart or the ionization frequency. The anomalous electron collision frequency is in quantitative agreement (within a factor of 3) with the inferred collision frequency due to the presence of IAT. This result agrees with numerical simulations of hollow cathodes that include the effect of enhanced electron drag from turbulence. In light of these encouraging results, we continue our analysis in the time domain to determine, as others have suggested that time-variations in the electron resistivity are the result in oscillations in the turbulent wave energy.

B. Time-resolved Anomalous Resistivity and High-frequency Turbulence

Moving to our primary novel contribution in this work, we examine the relationship of the collision frequency to turbulence-driven drag on electron in the time domain. For this comparison, we use a time-resolved analysis of the probe measurements along with Eqns. 1 - 14 to determine the fluctuations in the electron collision frequency. We also calculate the effective collision frequency due to IAT by determining how the amplitude of these modes change in time.

To measure the time-resolved collision frequency, we must first correlate all of our measurements of the plasma parameters. We conduct a phase-average of the high-speed plasma potential, floating potential, and ion saturation current measurements, using the discharge current as a consistent reference signal. This is accomplished by first bandpass filtering the discharge current signal with a lower cutoff frequency of 30 kHz and an upper cutoff frequency 100 kHz and

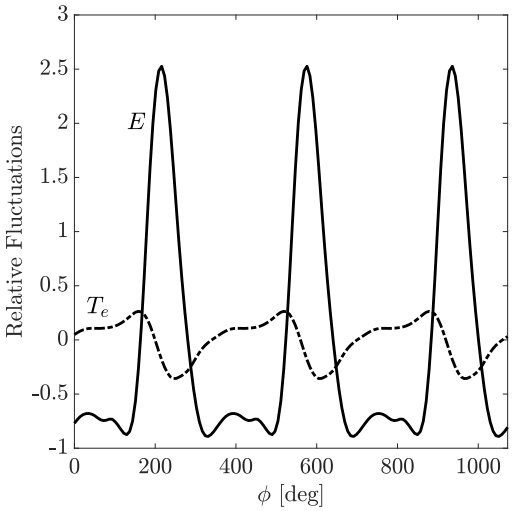

(a) Electric field and Temperature fluctuations at z = 5 mm.

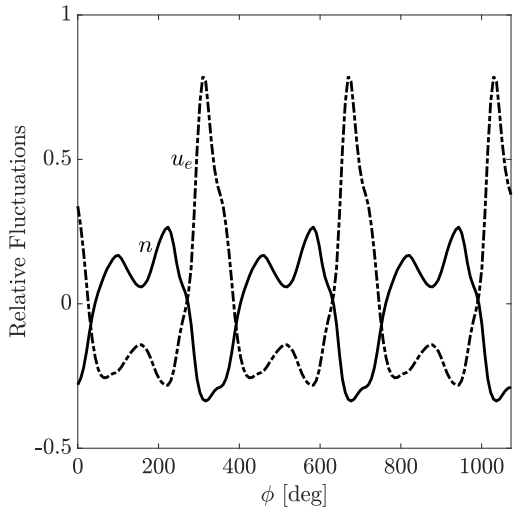

(b) Density and velocity fluctuations at z = 5 mm.

Fig. 5 Time-resolved plasma parameters.

searching for peaks. Because the frequency of the plume mode oscillation is not steady, the time between peaks may vary. As such, we average in phase space, assuming that the processes behind the oscillation consistent over a cycle. We split the phase into 50 bins from 0° to 360° (each bin containing about 4-6 points in time) and average over 4000 cycles to recover the phase-averaged signal. Using Eqns. 10 - 14, we estimate the relative fluctuations of the plasma parameters. Figure 5a shows the oscillations in electric field and electron temperature and Fig.5b similarly shows the time-resolved density and velocity perturbuations. Here, we see that the electric field is about 60 degrees out of phase with the electron temperature and that the density and velocity are completely out of phase. We note that at certain locations in the plume, our time-resolved analysis resulted in a plasma density that was temporarily negative. This is indicative of the probe collecting electrons, not ions. As a result, we have removed these spurious points from our time-resolved analysis.

We evaluate Eqn. 1 with these plasma parameters to calculate the anomalous contribution to the electron collision frequency. On the other hand, to calculate the effective collision frequency from turbulence over time, we must use a phase-averaged Fourier transform and summing over the IAT modes. The procedure for this is discussed in Ref. [20] and a similar analysis can be found in Ref. [28]. In brief, we calculate the Fourier transform over a short window, relative to the plume mode oscillation. The window is translated in time to capture 10 distinct phases of the cycle and averaged over 5000 cycles. This choice of window provides sufficient temporal and spectral resolution to resolve any changes in the amplitude of the IAT modes over time.

Figure 6 shows the response of the relative fluctuations in the total collision frequency to the classical and anomalous components at z = 5 [mm]. The response curve is generated by plotting a time-varying parameter, in this case the total electron collision frequency, against another, such as the classical or anomalous collision frequency. Two parameters that are highly correlated will produce a straight line with a slope of 1, where as poorly correlated properties will generate some curve. in Fig. 6, we see that the total electron frequency is highly correlated with the total collision frequency, as indicated by the linear relationship between $\tilde{\nu}$ and $\tilde{\nu}_{an}$. The classical collision frequency, on the other hand, is uncorrelated with the total collision frequency. Ultimately Fig. 6, serves to show that the time dependence of the total collision frequency is highly correlated with and largely dictated by the anomalous component.

Figure 7a shows the fluctuation of the anomalous collision frequency relative to its mean as calculated from Eqns. 1 and 6, as well as the classical collision frequency (Eqn. 2). We have concatenated three cycles of oscillation to better show the structure. The uncertainty in our measurement is derived from the standard deviation along the vertical axis the bin width in the horizontal axis. Within the uncertainty of the measurement (±16°), the fluctuations depicted in

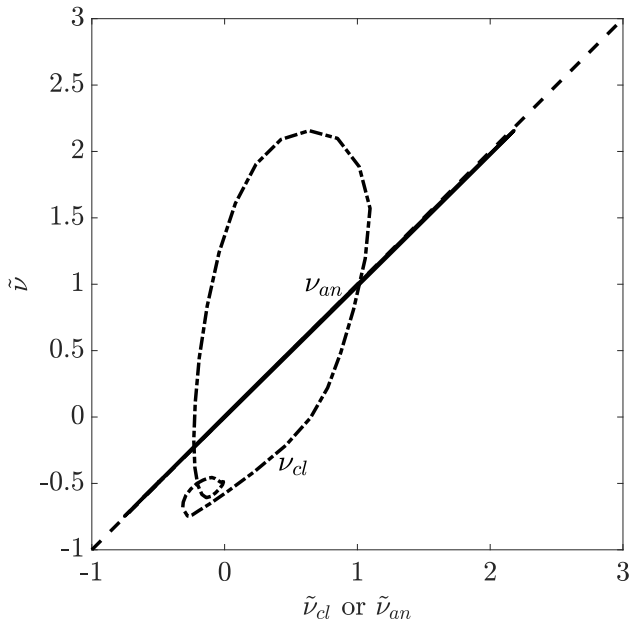

Fig. 6 Response curve of the electron collision frequency to the classical and anomalous collision frequencies.

Fig. 7a are in quantitative agreement. We find similar agreement between 0.5 to 0.8 cm from the cathode; however, further downstream, as shown by the representative plot in Fig. 7b, there is a stark difference in the waveforms that is discussed in the following section. The classical collision frequency is slightly out of phase with the anomalous collision frequency, has a lower relative amplitude is only moderately correlated with the total collision frequency. The response curve in Fig. 7c shows that the wave-driven collisions are relatively well correlated with the total collision frequency at $z = 5$ mm, barring some small phase off set producing the relatively circular shape in the response curve. At $z = 17$ mm, however, we find that these two parameters are not correlated. The results in Fig. 7c, ulimately reiterate our findings in Figs. 7a and 7b that the fluctuations in plasma resistivity are only well described by oscillations in wave-driven drag near the cathode.

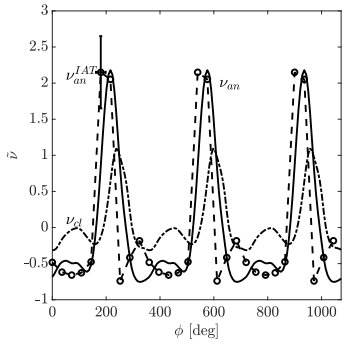

(a) Time-resolved relative fluctuations of the measured collision frequency and the wave-induced collision frequency from ion acoustic turbulence. $z = 5$ mm.

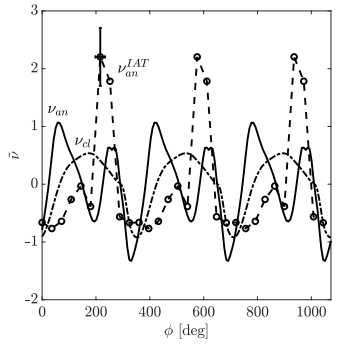

(b) Time-resolved relative fluctuations of the measured collision frequency and the wave-induced collision frequency from ion acoustic turbulence. $z = 17$ mm.

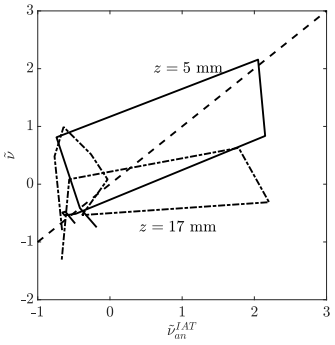

(c) Response curve of the electron collision frequency to the wave-driven collision frequency.

Fig. 7 Time resolved wave properties.

VI. Discussion

Our results strongly indicate that high-frequency turbulence is responsible for the apparent enhanced collisionality in the cathode plume during plume mode operation. And most notably in the near cathode region (0.5 - 0.8 cm), our measurements of high-frequency turbulence show that they dictate the fluctuations in the total electron collision frequency. Qualitatively, our results agree with observations from numerical simulations of hollow cathodes in plume mode [8, 9], where the large-scale oscillations are tied to the presence of an enhanced resistivity from IAT. Examining this connection more quantitatively through the closure models in Eqns. 7 and 8, we show in Fig. 8 that these models are not highly correlated with the fluctuations in total collision frequency. In particular, the amplitude of the oscillations predicted by Eqn. 7 are an order of magnitude smaller than those observed in our experiment, indicated by the curve being almost entirely in the $\tilde{\nu}$ direction. On the other hand, the closure in Eqn. 8 is on the same order of magnitude as our observations, however is not in phase. This is perhaps because we have neglected the convective term in Eqn. 8. These results indicate that perhaps a saturated model of the turbulence may not be sufficient to properly recover the oscillations in the turbulence-driven resistivity. Furthermore, this suggests that we may need to consider the time-variation of the turbulent wave energy to determine an accurate onset criterion for this mode.

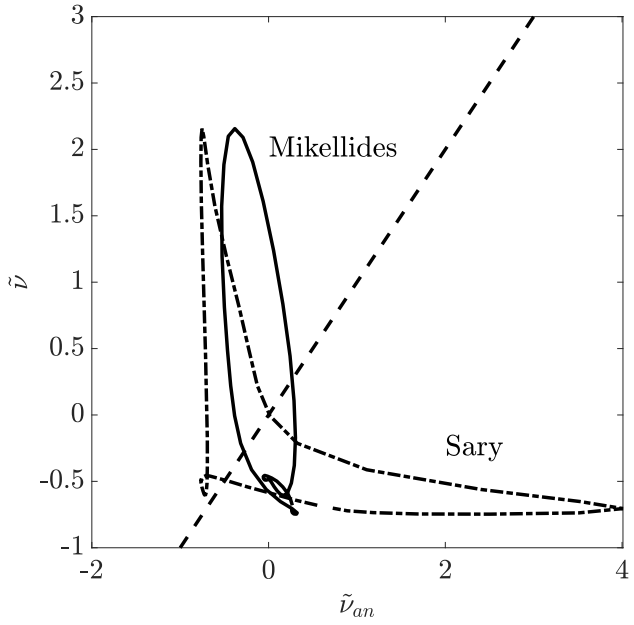

Fig. 8 Response of the total collision frequency to the anomalous collision frequency calculated from the closure models in Eqns. 7 and 8.

Physically, our results in the context of those in the literature [8, 9, 20] suggest the following possible oscillation mechanism. Heating from the increased resistivity leads to high electron temperatures and ionization. In response, the plasma increases the density to reduce the electron velocity. Since the growth rate of the IAT is approximately given by

$$\gamma_k = k c_s \frac{u_e}{v_e}, \tag{15}$$

where c_s is the ion sound speed, and v_e is the electron thermal speed, the lower electron velocity and increased temperature reduce the growth of the turbulence. This, in turn, reduces the heating of electrons. Through this possible mechanism, we would also expect the characteristic fluctuations in light emission as a result of the varying temperature. This is corroborated by our measurements of the peak-peak electron temperature fluctuations, depicted in Fig. 9, which exhibit a maximum downstream of the cathode and decreasing amplitude towards the anode.

Although we have now established the important role of IAT in driving the fluctuations in plasma resistivity, a critical open question about this instability is the determination of an analytical onset criterion providing new physical insight. Without this information, predicting its onset on orbit or after 10 khrs of operation in deep-space may prove challenging. The experimental and numerical evidence points to the onset of IAT and the resulting heating as a driver for this instability; however, a clear interpretation corroborated with experimental evidence for why the presence of turbulence might lead to instability remains elusive.

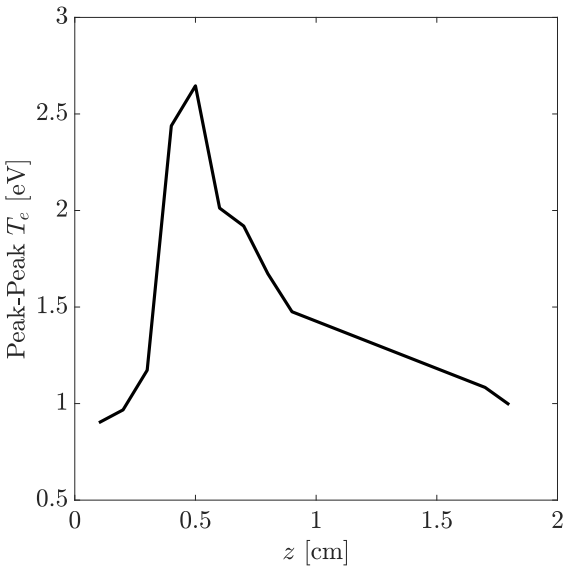

Fig. 9 Peak-peak temperature fluctuations.

VII. Conclusion

In conclusion, we have measured the collision frequency for electrons in space and time for the plume of a hollow cathode operating in plume mode and shown it to be driven primarily by non-classical behavior. Measurements of high-frequency turbulence commonly associated with ion acoustic turbulence are used to calculate an effective, anomalous collision frequency that proves to be in quantitative agreement with the observed collision frequency. Notably, near the cathode, we find that the fluctuations of these parameters in time are highly correlated in phase and amplitude; however, further downstream a more accurate estimation of the IAT growth rate may be necessary to find similar agreement. This evidence supports the notion that turbulence plays a critical role in the steady state properties as well as the temporal oscillation of the plasma in the plume mode, notably near the cathode. Upon examining our measurement in the context of the closures used in cathode simulations, we find that a saturated approximation does not appear sufficient to describe the amplitude of the oscillation in resitivity, and that likely a growing, time-varying turbulent wave energy may be necessary to produce realistic fluctuation levels. Ultimately, these results have direct bearing on the ultimate goal of deriving stability criterion for the onset of this oscillation and indicates that fluctuations in wave-driven, effective collisions plays a dominant role in the time-varying total electron collision frequency.

Acknowledgments

This work was funded by the National Aeronautics and Space Administration Space Technology Research Fellowship grant number NNX15AQ37H.

References

[1] Mandell, M., and Katz, I., "Theory of hollow operation in spot and plume modes," American Institute of Aeronautics and Astronautics, 1994. doi:10.2514/6.1994-3134, URL http://arc.aiaa.org/doi/10.2514/6.1994-3134.

[2] Mikellides, I. G., Katz, I., Goebel, D. M., Jameson, K. K., and Polk, J. E., "Wear mechanisms in electron sources for ion propulsion, II: Discharge hollow cathode," *Journal of Propulsion and Power*, Vol. 24, No. 4, 2008, pp. 866–879. URL http://arc.aiaa.org/doi/pdf/10.2514/1.33462.

[3] Goebel, D. M., Jameson, K. K., Katz, I., and Mikellides, I. G., "Potential fluctuations and energetic ion production in hollow cathode discharges," *Physics of Plasmas (1994-present)*, Vol. 14, No. 10, 2007, p. 103508. doi:10.1063/1.2784460, URL http://scitation.aip.org/content/aip/journal/pop/14/10/10.1063/1.2784460.

[4] Jorns, B. A., Mikellides, I. G., and Goebel, D. M., "Ion acoustic turbulence in a 100-A LaB6 hollow cathode," *Physical*

Review E, Vol. 90, No. 6, 2014, p. 063106. doi:10.1103/PhysRevE.90.063106, URL http://link.aps.org/doi/10.1103/PhysRevE.90.063106.

[5] Lopez Ortega, A., Mikellides, I. G., and Jorns, B., "First-principles modeling of the IAT-driven anomalous resistivity in hollow cathode discharges II: Numerical simulations and comparison with measurements," American Institute of Aeronautics and Astronautics, 2016. doi:10.2514/6.2016-4627, URL http://arc.aiaa.org/doi/10.2514/6.2016-4627.

[6] Jorns, B. A., Dodson, C., Goebel, D. M., and Wirz, R., "Propagation of ion acoustic wave energy in the plume of a high-current LaB6 hollow cathode," *Physical Review E*, Vol. 96, No. 2, 2017, p. 023208. doi:10.1103/PhysRevE.96.023208, URL https://link.aps.org/doi/10.1103/PhysRevE.96.023208.

[7] Sary, G., Garrigues, L., and Boeuf, J.-P., "Hollow cathode modeling: I. A coupled plasma thermal two-dimensional model," *Plasma Sources Science and Technology*, Vol. 26, No. 5, 2017, p. 055007. doi:10.1088/1361-6595/aa6217, URL http://stacks.iop.org/0963-0252/26/i=5/a=055007.

[8] Sary, G., Garrigues, L., and Boeuf, J.-P., "Hollow cathode modeling: II. Physical analysis and parametric study," *Plasma Sources Science and Technology*, Vol. 26, No. 5, 2017, p. 055008. doi:10.1088/1361-6595/aa6210, URL http://stacks.iop.org/0963-0252/26/i=5/a=055008.

[9] Mikellides, I. G., Guerrero, P., Lopez Ortega, A., and Polk, J. E., "Spot-to-plume Mode Transition Investigations in the HERMeS Hollow Cathode Discharge Using Coupled 2-D Axisymmetric Plasma-Thermal Simulations," American Institute of Aeronautics and Astronautics, 2018. doi:10.2514/6.2018-4722, URL https://arc.aiaa.org/doi/10.2514/6.2018-4722.

[10] Dodson, C. A., Perez-Grande, D., Jorns, B. A., Goebel, D. M., and Wirz, R. E., "Ion Heating Measurements on the Centerline of a High-Current Hollow Cathode Plume," *Journal of Propulsion and Power*, Vol. 34, No. 5, 2018, pp. 1225–1234. doi:10.2514/1.B36788, URL https://doi.org/10.2514/1.B36788.

[11] Stix, T. H., *The Theory of Plasma Waves*, 1962. URL http://adsabs.harvard.edu/abs/1962tpw..book.....S.

[12] Davidson, R. C., and Krall, N. A., "Anomalous transport in high-temperature plasmas with applications to solenoidal fusion systems," *Nuclear Fusion*, Vol. 17, No. 6, 1977, p. 1313. doi:10.1088/0029-5515/17/6/017, URL http://stacks.iop.org/0029-5515/17/i=6/a=017.

[13] Sagdeev, R. Z., and Galeev, A. A., *Nonlinear Plasma Theory*, 1969. URL http://adsabs.harvard.edu/abs/1969npt..book.....S.

[14] Csiky, G. A., "Measurements of some properties of a discharge from a hollow cathode," *NASA Technical Note*, 1969. URL https://ntrs.nasa.gov/archive/nasa/casi.ntrs.nasa.gov/19690008515.pdf.

[15] Philip, C., "A Study of Hollow Cathode Discharge Characteristics," *AIAA Journal*, Vol. 9, No. 11, 1971, pp. 2191–2196. doi:10.2514/3.50024, URL http://arc.aiaa.org/doi/10.2514/3.50024.

[16] Friedly, V. J., and Wilbur, P. J., "High current hollow cathode phenomena," *Journal of Propulsion and Power*, Vol. 8, No. 3, 1992, pp. 635–643. doi:10.2514/3.23526, URL http://dx.doi.org/10.2514/3.23526.

[17] Georgin, M. P., Jorns, B. A., and Gallimore, A. D., "An Experimental and Theoretical Study of Hollow Cathode Plume Mode Oscillations," Electric Rocket Propulsion Society, Atlanta Georgia, 2017.

[18] Georgin, M. P., Jorns, B. A., and Gallimore, A. D., "Experimental Evidence for Ion Acoustic Solitons in the Plume of a Hollow Cathode," Sevilla, Spain, 2018, p. 12.

[19] Georgin, M. P., Jorns, B. A., and Gallimore, A., "Plasma Instabilities in the Plume of a Hollow Cathode," *2018 Joint Propulsion Conference*, American Institute of Aeronautics and Astronautics, Cincinnati, Ohio, 2018. doi:10.2514/6.2018-4427, URL https://arc.aiaa.org/doi/10.2514/6.2018-4427.

[20] Georgin, M. P., Jorns, B. A., and Gallimore, A. D., "Correlation of ion acoustic turbulence with self-organization in a low-temperature plasma," *Physics of Plasmas -Submitted*, 2019.

[21] Jorns, B. A., Mikellides, I. G., and Goebel, D. M., "Investigation of Energetic Ions in a 100-A Hollow Cathode," *50th AIAA/ASME/SAE/ASEE Joint Propulsion Conference*, 2014, p. 3826. URL http://arc.aiaa.org/doi/pdf/10.2514/6.2014-3826.

[22] Huba, J. D., *NRL Plasma Formulary*, The Office of Naval Research, 2016.

[23] Subramanian, K. P., and Kumar, V., "Total electron scattering cross sections for argon, krypton and xenon at low electron energies," *Journal of Physics B: Atomic and Molecular Physics*, Vol. 20, No. 20, 1987, pp. 5505–5515. doi:10.1088/0022-3700/20/20/026, URL https://doi.org/10.1088%2F0022-3700%2F20%2F20%2F026.

[24] Jorns, B., Lopez Ortega, A., and Mikellides, I. G., "First-principles Modelling of the IAT-driven Anomalous Resistivity in Hollow Cathode Discharges I: Theory," American Institute of Aeronautics and Astronautics, 2016. doi:10.2514/6.2016-4626, URL http://arc.aiaa.org/doi/10.2514/6.2016-4626.

[25] Mikellides, I. G., Katz, I., Goebel, D. M., and Jameson, K. K., "Evidence of nonclassical plasma transport in hollow cathodes for electric propulsion," *Journal of Applied Physics*, Vol. 101, No. 6, 2007, p. 063301. doi:10.1063/1.2710763, URL http://aip.scitation.org/doi/abs/10.1063/1.2710763.

[26] Jorns, B. A., and Hofer, R. R., "Plasma oscillations in a 6-kW magnetically shielded Hall thruster," *Physics of Plasmas (1994-present)*, Vol. 21, No. 5, 2014, p. 053512. doi:10.1063/1.4879819, URL http://scitation.aip.org/content/aip/journal/pop/21/5/10.1063/1.4879819.

[27] Goebel, D. M., and Katz, I., *Fundamentals of electric propulsion: ion and Hall thrusters*, Vol. 1, John Wiley & Sons, 2008. URL http://books.google.com/books?hl=en&lr=&id=P5OGFXcBKcwC&oi=fnd&pg=PR5&dq=%22Electrode+Breakdown%22+%226:+Hollow%22+%22Ionization+Length+and+Scaling%22+%22Dielectric-Wall+Versus+Metallic-Wall+Comparison%22+%22Dispenser+Cathodes+in+Insert%22+%22Hall+Thruster%22+%22Pyrolytic+Graphite%22+%22Hollow+Cathode+Operation%22+%22TAL+Hall+Thruster+Efficiency+(Metallic+Walls&ots=Sbv2zvFn6h&sig=jItSQOscncTmqCz26jx_rAYmlbc.

[28] Tsikata, S., and Minea, T., "Modulated Electron Cyclotron Drift Instability in a High-Power Pulsed Magnetron Discharge," *Physical Review Letters*, Vol. 114, No. 18, 2015, p. 185001. doi:10.1103/PhysRevLett.114.185001, URL https://link.aps.org/doi/10.1103/PhysRevLett.114.185001.